Lawrence Berkeley National Laboratory

Title
Intermediates and the folding of proteins L and G

Permalink
https://escholarship.org/uc/item/0fd578jk

Authors
Brown, Scott
Head-Gordon, Teresa

Publication Date
2008-05-16

Title: Intermediates and the Folding of Proteins L and G

Authors: Scott Brown[†] and Teresa Head-Gordon*
Department of Bioengineering
University of California, Berkeley
Berkeley, CA 94720

Abstract. We use a minimalist protein model, in combination with a sequence design strategy, to determine differences in primary structure for proteins L and G that are responsible for the two proteins folding through distinctly different folding mechanisms. We find that the folding of proteins L and G are consistent with a nucleation-condensation mechanism, each of which is described as helix-assisted β−1 and β−2 hairpin formation, respectively. We determine that the model for protein G exhibits an early intermediate that precedes the rate-limiting barrier of folding and which draws together misaligned secondary structure elements that are stabilized by hydrophobic core contacts involving the third β−strand, and presages the later transition state in which the correct strand alignment of these same secondary structure elements is restored. Finally the validity of the targeted intermediate ensemble for protein G was analyzed by fitting the kinetic data to a two-step first order reversible reaction, proving that protein G folding involves an on-pathway early intermediate, and should be populated and therefore observable by experiment.
[†]Current address: Abbott Laboratories, 1401 Sheridan Road, North Chicago, Illinois 60064-4000

Introduction

While thermodynamics and kinetics of small proteins that fold via a two-state manner are reasonably well-understood (Daggett & Fersht, 2003a; Gruebele, 2002b; Myers & Oas, 2002), understanding how (and why!) proteins fold through intermediates will be especially relevant for larger proteins, more complicated topologies, and their possible connection to aggregation processes that are responsible for disease(Speed et al., 1997). Some of the open questions surrounding intermediates include the detection of the so-called "hidden" intermediates by kinetic experiments, whether intermediates can occur earlier than the rate-limiting step in folding, i.e. do free energy barriers that precede the rate-limiting nucleation barrier of the folding reaction exist, and if they are "off-pathway" and therefore obstruct the functionally important progress of folding (Gruebele, 2002a; Ozkan et al., 2002; Qin et al., 2002; Sanchez & Kiefhaber, 2003a).

This work examines the question of intermediates by simulating the folding of two members of the ubiquitin fold class, Ig-binding proteins L and G. Proteins L and G make excellent targets for theoretical study as their folding attributes have been extensively studied by experiment (Gu et al., 1997; Gu et al., 1995; Kim et al., 2000; Krantz et al., 2002; McCallister et al., 2000; Park et al., 1997; Park et al., 1999; Scalley et al., 1997). These two single-domain proteins have little sequence identity and but identical fold topologies, consisting of a central α−helix packed against a four-strand β−sheet composed of two β−hairpins. Experimental evidence indicates that protein L folds in a two-state manner through a

transition state ensemble involving a native-like β-hairpin 1, and largely disrupted β-hairpin 2(Gu et al., 1997; Kim et al., 2000; Scalley et al., 1997). Protein G on the other hand, folds through a possible early intermediate (Park et al., 1997; Park et al., 1999; Speed et al., 1997), followed by a rate-limiting step that involves formation of β-hairpin 2. They therefore provide a perfect contrast to understand features that give rise to protein folding intermediates, while controlling for size and topology.

There have been a number of recent simulations of coarse-grained models of proteins L and/or G using different forms of minimalist models(Head-Gordon & Brown, 2003). Shimada and Shakhnovich have used ensemble dynamics to characterize the kinetics of protein G using an all-atom Gō potential(Shimada & Shakhnovich, 2002). Karanicolas and Brooks use a Gō potential bead model supplemented with sequence-dependent MJ statistical potentials to differentiate the folding of G and L(Karanicolas & Brooks, 2002). They found the origin of asymmetry in the folding of protein L and G to be in concurrence with that found by Nauli and co-workers (Nauli et al., 2001), who used a computer-based design strategy to reengineer the protein G sequence to include more stabilizing interactions for the first beta-hairpin turn, producing a protein more faithful to the mechanism of folding for protein L.

Our recent work, inspired by early efforts of Thirumalai and co-workers (Guo & Thirumalai, 1996; Guo et al., 1992; Honeycutt & Thirumalai, 1990), develops physics-based potentials which make the connection between free energy landscapes and amino acid sequence, allowing us to engineer sequences that

fold into α–helical, β–sheet, and mixed α/β protein topologies(Brown et al., 2003; Sorensen & Head-Gordon, 2002; Sorenson & Head-Gordon, 1999; Sorenson & Head-Gordon, 2000; Sorenson & Head-Gordon, 2002). These coarse-grained protein models provide the right emphasis of the most relevant native state features (Head-Gordon & Brown, 2003) by capturing the correct spatial distribution of local and non-local contacts which are considered to be possibly the most important in governing the overall kinetics of protein folding (Alm et al., 2002; Plaxco et al., 1998). We have previously explored its use for members of the ubiquitin α/β fold class including proteins L and G and ubiquitin (Brown et al., 2003; Sorensen & Head-Gordon, 2002; Sorenson & Head-Gordon, 2000; Sorenson & Head-Gordon, 2002). Recently we have verified that the use of a three-letter sequence code is capable of translating the differences in primary sequence for proteins L and G into the experimentally observed differences in thermodynamic and kinetic properties of folding(Head-Gordon & Brown, 2003).

In this work, we analyze the kinetics of folding for these distinct sequences in order to characterize the dynamics of navigating the free-energy landscape from unfolded to native state. P_{fold} simulations (Du et al., 1998) and contact map analysis of have been used to characterize the folding landscape. The folding of our protein L model follows two-state kinetics, and shows the presence of a transition state ensemble with a well-formed β–hairpin 1. Similar analysis of protein G shows that it folds through at least two pathways, which we label the fast and slow pathways. The fast pathway exhibits two-state kinetics and folds through a transition-state ensemble with a well-formed β–hairpin 2. In both cases of protein L and fast folding protein G, these secondary structural elements are assisted by the α–helix, and the overall folding mechanism seems consistent with a nucleation-condensation mechanism observed for other proteins (Daggett & Fersht, 2003a; Daggett & Fersht, 2003b).

The slow pathway for protein G is what gives rise to three-state kinetics, and involves an early intermediate, i.e. an intermediate that precedes the rate-limiting step in folding. The characteristics of the intermediate are hydrophobic contacts involving the third β–strand interacting with β–strands 1 and 2, although the associated secondary structure strand elements are misaligned relative to our model of the folded state. The transition state that occurs after the intermediate and proceeding the folding to the native state is characterized by native-like registering of these same β–strand pairings. The tractability of the simulation model allows us to fit the kinetic data to a unimolecular two-step kinetic model to summarily characterize the kinetics of protein G folding. We

confirm that a barrier in fact separates the unfolded state from the early folding intermediate, and is lower in free energy relative to the unfolded state, so that the intermediate should be populated and observable by experiment.

Results

One of the differences between our L and G model proteins is manifested in the relative thermodynamic stability of the different elements of secondary structure. Figure 1 shows free-energy projections along $\chi_{\beta 1}$ and $\chi_{\beta 2}$ for L and G.
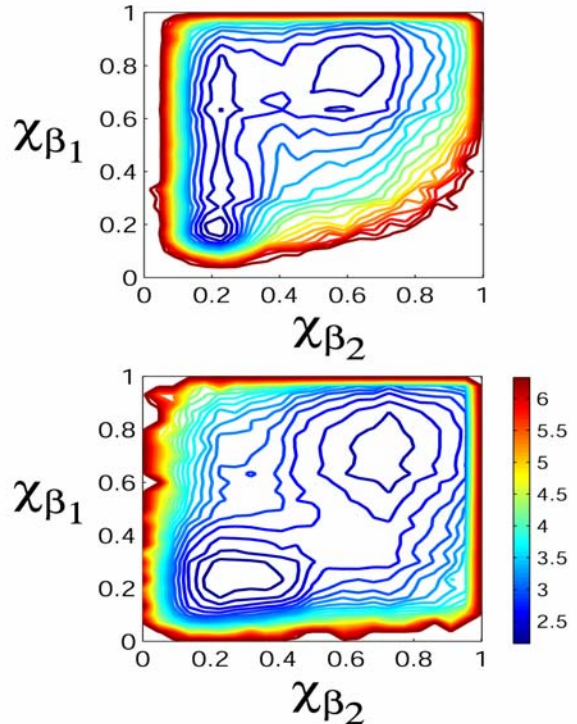

Figure 1: Free-energy projections onto order parameters $\chi_{\beta 1}$ and $\chi_{\beta 2}$ for L and G. a) Free-energy contour plot for protein L as a function of native-state similarity of the second (C-terminal) β-sheet region $\chi_{\beta 2}$ and first (N-terminal) β-sheet region $\chi_{\beta 1}$ at the folding temperature. Note the minimum free-energy path connecting the unfolded and folded ensembles proceeds through a transition state in which the β_1 region is native and the β_2 region is largely disrupted. b) Free-energy contour plot for protein G as a function of native-state similarity of the second (C-terminal) β-sheet region $\chi_{\beta 2}$ and first (N-terminal) β-sheet region $\chi_{\beta 1}$ at the folding temperature. For G, the minimum free-energy path connecting the unfolded and folded ensembles proceeds through a transition state in which the β_2 region is native-like and the β_1 region is disrupted. Contour lines are spaced $k_B T$ apart.

From these projections there is a minimum free-energy path connecting the unfolded ensemble to the folded ensemble that involves either sequential formation of β-hairpin 1 followed by β-hairpin 2 (protein L), or β-hairpin 2 followed by β-hairpin 1 (protein G). However, we appear to only be getting

part of the picture in Figure 1, as the barrier height separating the unfolded and folded ensembles is insufficiently high (relative to k_BT) to justify locating the rate-limiting transition state solely on this surface.

The folding kinetics at the folding temperature, shown in Figure 2, illustrates the difference in folding mechanism between L and G (fit parameters given in Table 1). The kinetic data for protein L is fit well by a single-exponential, consistent with what is reported in the literature for protein L(Kim et al., 2000; Scalley et al., 1997). Thus our protein L model folds in a cooperative two-state manner, and possibly through the initial formation of β-hairpin 1.

For protein G the story is not as straightforward. We find that protein G folds slower than protein L by a factor of two, qualitatively consistent with experiment (McCallister et al., 2000); however, the kinetic data for protein G is better fit by at least a double exponential (parameters shown in Table 1).
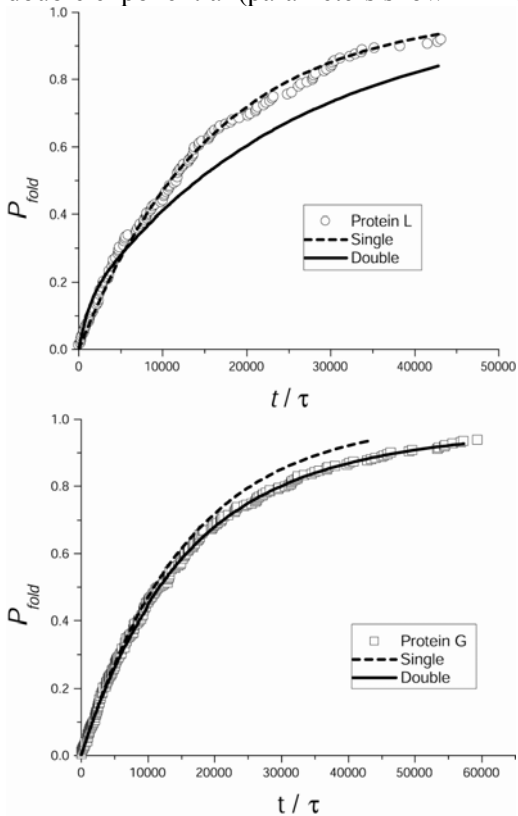

Figure 2: Folding kinetics for proteins L and G. a) Fraction of folded states P_{fold} as a function of time t for protein L at the folding temperature. The best fit to the data is by a single exponential. b) Fraction of folded states P_{fold} as a function of time t for protein G at its folding temperature. The best fit for this data is to a double exponential. All fit parameters are given in Table II.

Table 1. Parameters obtained from fits to kinetic data. The data is fit to the equation: $A_0 \exp(-t/\tau_0) + (1-A_0) \exp(-t/\tau_1)$

	T	A_0	$1-A_0$	τ_0	τ_1	$\chi^2 / 10^{-4}$
L	0.42	1.0	0	15700	0	3.43
G	0.41	0.81	0.19	13700	46400	0.353

From this fit we find two populations, one involves a fast folding event in which roughly 80% of the population folds cooperatively, and a slow folding remainder of the ensemble that folds by a different mechanism that we analyze further below. The time scale that serves to roughly delineate these two populations is 2×10^6 time steps. After this many time steps the majority of the fast folding states have folded, while only a tiny fraction of the slow folders have folded. Using 2×10^6 time steps as a cutoff, we refit the kinetic data of the fast-pathway population for protein G and obtain a single exponential, while the fit to the remaining 20% of slow folders gives a double exponential, suggestive of an intermediate state in the slow folding trajectories.

If we examine the folding ensemble at both early and late times for the two populations, we see that the fast pathway involves a collapse concomitant with folding scenario (Figure 3a). The fast pathway also involves a greater degree of native α-helix formation relative to the slower population. This is an important difference between the two pathways, and we will return to it later. The slower population is characterized by more relative ordering of both β-sheet regions 1 and 2 (Figure 3b). Note that both kinetic pathways exhibit a more developed β_2 region relative to the β_1 region, reflecting what is seen in the thermodynamic analysis. The picture from both kinetics and thermodynamics appears to be consistent and points to a folding mechanism that involves formation of β-hairpin 2 at some rate-limiting step prior to that of β-hairpin 1.

Shown in Figure 4 is a two-dimensional free-energy surface projected onto the radius of gyration, R_g, and native-state similarity parameter, χ. Figure 4a shows the relationship between L collapse and native-state formation, which appears to occur by a single pathway leading from expanded, non-native to the minimum on the surface corresponding to collapsed and native-like. This is consistent with
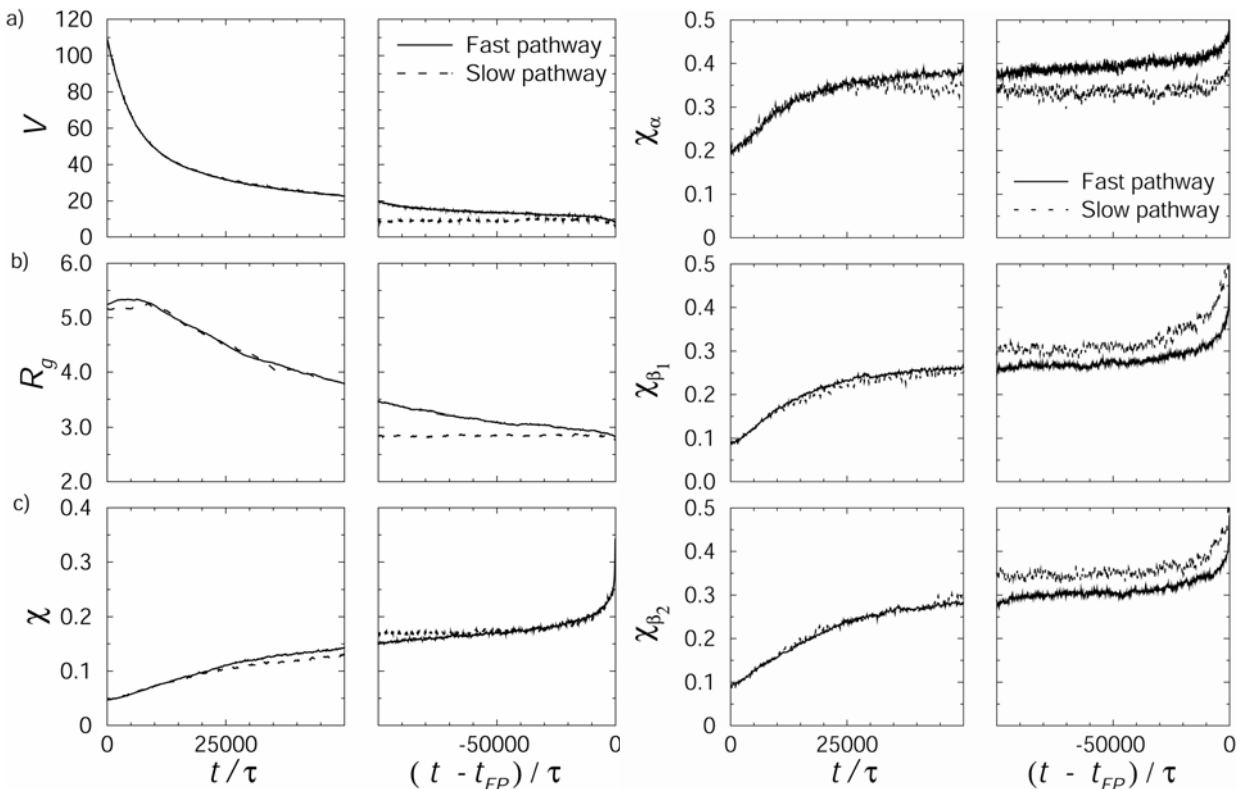
Figure 3: Shows the presence of two folding pathways for protein G. (a) The fast pathway corresponds to a collapse concomitant with folding scenario, while (b) the slow pathway corresponds to non-productive collapse and a longer process of finding the native structure.

the picture from kinetic data of a collapse concomitant with folding scenario(Plaxco et al., 1999). In contrast to this, for protein G there appear to be two pathways for collapse, with two separate minima for each pathway, as illustrated by the arrows in Figure 4b. One pathway involves collapse to a largely non-native structure, whereas the other pathway reflects a collapse concomitant with folding scenario, as seen with protein L. The barrier separating these two minima in Figure 4b again has insufficient height to account for observed kinetic data.

Recent work has strongly emphasized that the choice of reaction coordinate for monitoring folding progress is important for the observation of intermediates and general interpretation of kinetic data (Qin et al., 2002). A potential pitfall of choosing a reaction coordinate is illustrated in Figure 5, which shows the potential of mean force for protein G as a function of native-state similarity in going from the unfolded ($\chi \approx 0$) to folded ($\chi \approx 1$) states for a range of temperatures spanning the folding temperature. In producing our kinetic data we use this same native-state similarity parameter to determine the extent of folding during folding trajectories. Note that the folding temperature for the protein G sequence is $T^* \approx 0.41$. Jumping from the free-energy surface at $T^* = 0.5$ to the surface at $T^* = 0.35$ would involve a downhill rearrangement in the distribution of the unfolded ensemble. These results represent an

alternative interpretation of ultra-fast folding experiments that remains consistent with overall evidence for two-state folding(Parker & Marqusee, 1999).

One of the benefits of coarse-grained models is the ability to fully characterize ensemble kinetics on the free energy landscape by investigating transition state ensembles, and putative intermediates, provided we can find suitable reaction coordinates for their description. We examined a number of reaction coordinates before determining ones that adequately capture the folding events in our model. These include contact order parameters α, β_1, β_2, $\beta_2\alpha$, $\beta_3\alpha$, $\beta_1\beta_2$, $\beta_1\beta_4$, $\beta_2\beta_3$, $\beta_3\beta_4$, $\beta_3\beta_4\alpha$, $\beta_2\beta_3\alpha$, $\beta_1\beta_2\beta_3$, as well as a "diffuse" order parameter that was an expanded native state.

Several additional folding-trajectory analyses were performed to obtain more extensive kinetic characterization, in which progress during folding was monitored along a variety of these chosen order parameters. Structures with desired values along these order parameters were saved and served to form a set of putative transition states, which were then subsequently used as starting structures in trajectories for P_{fold} analysis. From the P_{fold} simulations we obtained a subset of successful order parameters (shown in Table 2), which correlate well with the definition of transition state ensemble. Through this procedure we determined a transition state ensemble for protein L, a transition state ensemble for the fast

4

Table 2. Order parameters, *Q*, used for characterizing folding mechanisms in proteins L and G, along with contacts used to define them.

| Q	*i*th:*j*th Bead Contacts
Protein L Transition State	
$\beta_1\beta_2\alpha$	6:16 6:17 6:18 7:15 7:16 7:17 8:13 8:14: 8:15 8:16 8:17 9:1 9:14 9:15 10:14 10:15 20:24 23:27 29:33 30:34
Protein G Transition State (fast pathway)	
$\beta_3\beta_4\alpha$	10:14 20:24 20:27 23:27 24:28 27:31 36:53 36:54 36:55 37:53 38:52 38:53 39:51 41:48 41:50 41:51 42:48 42:49 43:47 43:48 43:49 44:48
Protein G Transition State (slow pathway)	
$\beta_1\beta_3\beta_2$	8:14 8:15 8:16 8:17 8:36 8:37 8:38 9:13 9:14 9:15 9:36 10:14 14:36 15:36 17:38 19:40 19:41 19:42 20:41 20:42 20:49 21:41 21:42 21:43 43:48
Protein G Intermediate	
$\beta_2\beta_3\alpha$	8:14 9:13 9:14 9:15 10:14 18:40 18:41 19:39 19:40 19:41 23:27 27:31 31:35 42:48 43:47 43:48 43:49 44:48
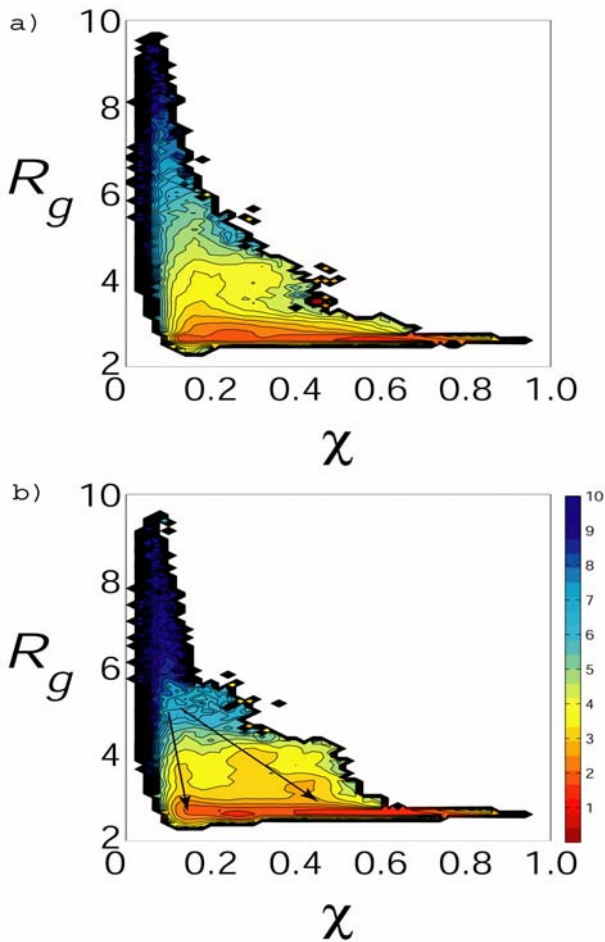
Figure 4: Free-energy surface projected onto order parameters R_g and χ. a) Free-energy contour plot for protein L as a function of radius of gyration R_g and native-state similarity χ. In this plot there is only a single dominant minimum that corresponds to a collapsed, largely native structure. b) Free-energy contour plot for protein G as a function of radius of gyration R_g and native-state similarity χ. In this plot there appear to be two dominant minima, one corresponding to collapsed non-native structures and the other to collapsed native-like structures.
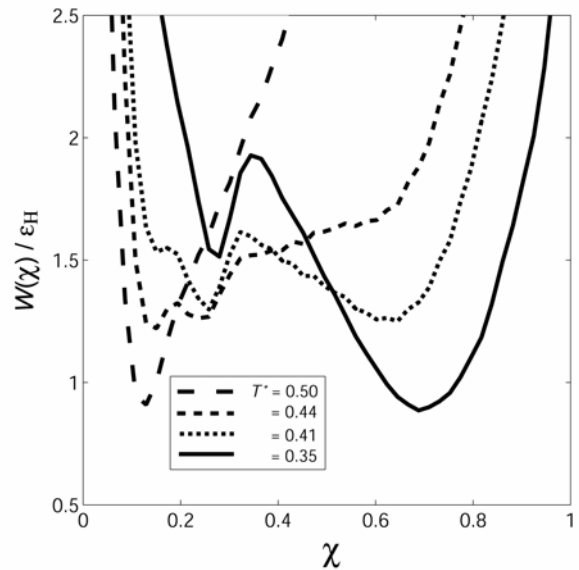

Figure 5: Potential of mean force vs. native state similarity as a function of temperature for protein G. The folding temperature is $T^* = 0.41$. Based on this projection we might conclude that there is a shift in the unfolded population as we approach folding conditions. There is also evidence for a small barrier.

pathway in protein G, and the late transition state ensemble for the slow folding pathway of protein G. During P_{fold} simulations the trajectories either fold or do not fold, by definition. By saving the structures for those trajectories that did *not* fold in the P_{fold} simulations of structures corresponding to the transition state ensemble of the slow folding pathway for protein G, we were able to isolate the structural characteristics of the ensemble of early intermediates. Figure 6a shows a contact map with reference lines indicating native-state contacts (black line) and the contacts that are present across at least 90% of the transition-state ensemble for protein L (gray line). The transition-state contacts show that the model for protein L folds through structures with a helix-assisted β−1 hairpin nucleus.
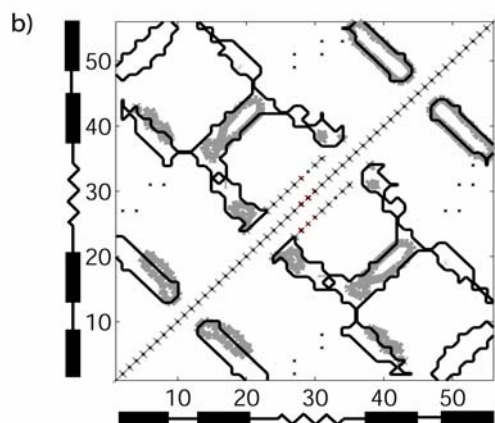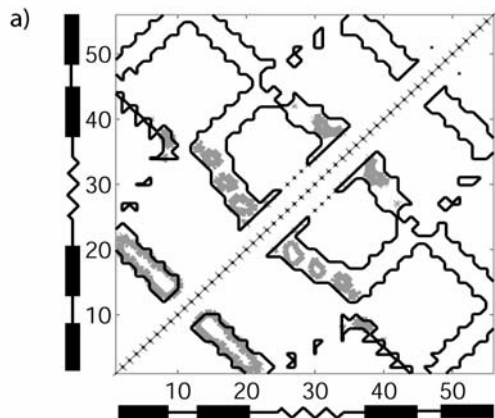
5

Figure 6: Contact map comparing native state (black) to contacts that are found present in the transition-state ensemble for 90% or greater of the structures (gray) for (a) protein L and (b) fast folding pathway of protein G.

Figure 6b shows a similar map of contacts to delineate the transition state ensemble in the fast pathway of protein G. In the case of protein G's fast pathway the transition-state ensemble involves formation of a helix-assisted β−2 hairpin nucleus.

Figure 7a shows the contact map for the contacts present in at least 90% of the structures in our intermediate ensemble. Figure 7b shows the contacts present in at least 90% of the late transition-state ensemble structures for the slow folding pathway of protein G. The intermediate is characterized by associated helix with β−strands 2 and 3, with a smaller amount of associated β−strands 1 and 3; however, these strands are misaligned relative to the native state. The subsequent transition state ensemble is in large part characterized by an alignment correction of this same strand association pattern exhibited in the intermediate, followed by more robust association of the other β−strands.
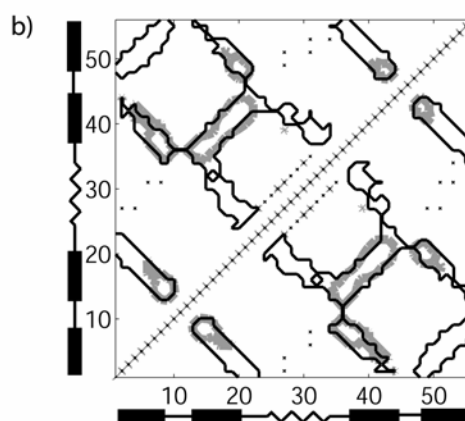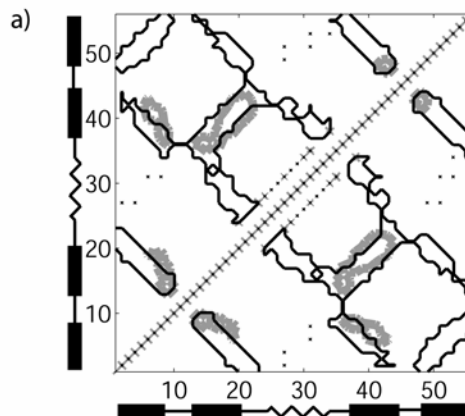
Figure 7: Contact map comparing native state (black) to contacts that are found present in the (a) intermediate ensemble and (b) transition-state ensemble, for 90% or greater of the structures for the slow folding pathway of protein G (gray).

Finally we prove that the intermediate occurs early on the pathway by fitting the data to a two-step reversible first order UIN mechanism. Given the characterization of the intermediate for the slow pathway of protein G, we can monitor individual folding trajectories and record when states enter and leave the U, I, and N designations. Provided we observe a large number of trajectories, we can assemble a picture of the pathway the folding population follows as a function of time, and fit the corresponding data to the UIN mechanism:

$$[U] \; \frac{k_1}{k_{-1}} \; [I] \; \frac{k_2}{k_{-2}} \; [N] \quad (1)$$
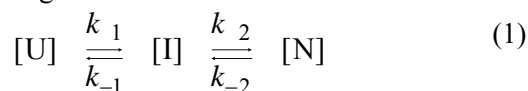
The solutions for the time rate of change of concentration of each species expressed as a function of rate constants k_1, k_{-1}, k_2, and k_{-2}, is given in Appendix I. As far as we are aware, this is the first time a solution of the full UIN mechanism without

6

simplifying approximations has appeared in the protein literature, although this mechanism is very often invoked in the analysis of protein folding reactions in its various simplified limiting forms. When our data is fit to these equations they yield values of the rate constants and associated estimates of relative free-energy minima, which are given in Table IV. We also show the quality of the fit of the slow folding protein G data to the UIN model in Figure 8.
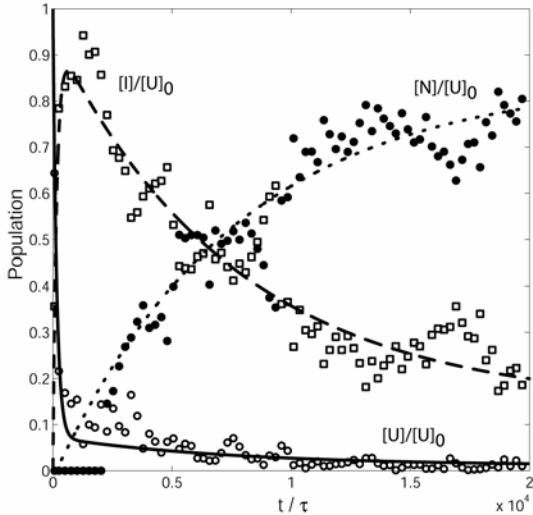

Figure 8: Kinetic data and fits for UIN folding mechanism scenario.

Note that in Figure 8 we have enforced a restriction in which we eliminate all trajectories that fold prior 2×10^6 time steps. This allows us to focus exclusively on the trajectories folding via the slow pathway, but leads to a slight anomaly in Figure 8 for the populations immediately prior to 2000τ. By removing greater than 95% of the fast folding trajectories we have excluded a small fraction of the slow folding trajectories. In summary, the kinetic model demonstrably shows that a barrier in fact separates the unfolded state from the early folding intermediate, and that the intermediate is lower in free energy relative to the unfolded state, and therefore should be populated and observable by experiment.

Conclusions
We find that protein L is a two-state folder, in agreement with existing experiments (Gu et al., 1997; Kim et al., 2000; Scalley et al., 1997). As such, it provides a unique reference system for understanding intermediates by comparing its folding to protein G, a structurally homologous protein of similar length for which continuous flow fluorescence experiments support the population of an early intermediate along the folding pathway (Park et al., 1997; Park et al., 1999). This by definition involves the presence of an

Table 3. Parameters obtained from fit to UIN kinetic model outlined in Appendix I to characterize the slow folding pathway of protein G.

k_1	k_{-1}	k_2	k_{-2}	$\Delta G_{U\text{-}I}$	$\Delta G_{I\text{-}N}$
1.1×10^{-3}	1.3×10^{-4}	2.3×10^{-5}	4.0×10^{-6}	$-2.0 k_B T$	$-1.7 k_B T$

additional free energy barrier preceding the rate-limiting barrier in folding. It is important to note that the stopped flow experiments cannot resolve any early intermediates in the folding of protein L, unlike the better time-resolved continuous flow experiments for protein G. While continuous flow results have been called into question as a problem of suspect interpretation of ultra-fast folding events in general (Krantz et al., 2002), our model supports the view that protein G folds through an early intermediate while protein L does not.

Protein L's transition state ensemble is composed of helix-assisted β−1 hairpin formation. We conclude that protein G folds through at least two pathways: a fast pathway involving roughly 80% of the folding population, with a transition state composed of a helix assisted β−2 hairpin nucleus, and a slow folding pathway through which the remaining folding population proceeds in a three-state mechanism. Our model clearly demonstrates that the slow pathway involves the presence of an early intermediate involving the third β−strand, that it is separated from the unfolded state by a significant barrier (relative to $k_B T$), and in fact is lower in free energy relative to the unfolded state (Table IV), and therefore should be populated and observable by experiment. Therefore our model strongly supports the interpretation of the continuous flow experiments by Park et al. (Park et al., 1997) as evidence of an early folding intermediate.

Our results also emphasize that the choice of reaction coordinate used experimentally is very important to avoid conflicting conclusions concerning the presence of intermediates, as was found to be the case for reexamination of the presence of an intermediate in ubiquitin. Similar conclusions concerning the proper determination of reaction coordinates that monitor folding was also found by Shimada and Shakhnovich(Shimada & Shakhnovich, 2002). Their simulation of protein G found that folding occurred through multiple pathways, each of which passes through an on-pathway intermediate. They showed that when folding is monitored by using burial of the lone tryptophan in protein G as the reaction coordinate, the ensemble kinetics shows a significant burst phase, while alternative reaction coordinates reveal the presence of different folding pathways. They make the point that ensemble averaging can mask the presence of multiple

pathways when non-ideal reaction coordinates are used. We required a variety of different order parameters, coupled with P_{fold} analysis, to characterize the reaction coordinates for protein L and protein G folding to find all intermediates and transition states. Furthermore we fit our kinetic data to a UIN type mechanism and provide estimates of the rate constants and relative free-energy minima to fully characterize the folding pathways.

The work reported by Shimada and Shakhnovich using an all-atom Go potential (Shimada & Shakhnovich, 2002) most closely parallels the study described here of analyzing the folding of protein G. They observe three pathways, each involving its own intermediate: I_1 (helix-hairpin 1), I_2 (helix-hairpin 2), and I_3 ($\beta1$-$\beta4$), and that each pathway converges to the same transition state. Our physics-based α-carbon trace model finds two major pathways each with its own transition-state, with only one pathway exhibiting an intermediate characterized by $\beta_2\beta_3\alpha$. At this point it is difficult to tell more about the structural nature of the experimental intermediate given the non-specific nature of the tryptophan (on the third β-stand) reaction coordinate used in the experimental study. However, we expect that the structural details of the intermediate are potentially more reliably predicted with the all-atom simulation since our coarse-grained model inadequately describes β-sheet structure, and instead forms a β-strand bundle for proteins L and G.

However, due to the inexpensive cost of our bead model, we are able to perform various analyses of thermodynamics as well as P_{fold} analyses along entire trajectories to isolate structures belonging to the transition-state and intermediate ensembles. This level of detailed investigation is not possible (or is not pursued) in more complicated models. For example, the total number of trajectories examined in (Shimada & Shakhnovich, 2002) is only 50, whereas we examine 1000 folding trajectories. With only 50 trajectories we found that we were unable to reliably analyze our data and make comment on ensemble folding properties. We found this to be a particularly significant problem when fitting to our postulated three-state reaction mechanism. The primary advantage of physics-based bead models is that the kinetics and thermodynamics are fully characterizable with high quality statistics, and the overall qualitative agreement with experiment is very good.

The differences in the folding properties of L and G, for the fast pathways, are consistent with a nucleation-condensation model (Abkevich et al., 1994) or nucleation-collapse mechanism (Guo & Thirumalai, 1995) that has been used to analyze kinetic data on two state folders (Daggett & Fersht, 2003a; Daggett & Fersht, 2003b; Fersht, 1997; Sanchez & Kiefhaber, 2003b). Whereas the fast pathway mechanisms for L and G involve the contact-assisted formation of secondary structure to create a folding nucleus at the transition state, the slow pathway in protein G involves an obligatory intermediate that precedes the rate limiting step, a result that may seem inconsistent with a nucleation-based mechanism. However, as is seen in the case of barnase(Daggett & Fersht, 2003a), the intermediate for protein G assists in formation of the folding nucleus. It has been pointed out that increasing the hydrophobicity may lead to a shift in folding mechanism towards a molten-globule-like intermediate(Daggett & Fersht, 2003a); that does not appear to be the case here. It should be noted that in this model the sequences for proteins L and G have an identical number of L and B beads, and thus have an identical global hydrophobicity. However, the third β-strand is significantly more hydrophobic in protein G relative to protein L, and hence the intermediate certainly arises due to stabilization by hydrophobic contacts.

This greater hydrophobicity for protein G helps stabilize an intermediate that draws together the secondary structure elements of β-strand 3 in association with β-strands 1 and 2, although these secondary structure elements are out of register relative to the native state. However, this helps set up the final step in folding which now involves a transition-state ensemble that corrects for the misalignment of this core nucleus of associated strand elements. Recent work has suggested that intermediates that are higher in free energy relative to the unfolded state (perhaps hidden from experimental view) can accelerate folding (Sanchez & Kiefhaber, 2003a; Wagner & Kiefhaber, 1999). Protein G folding involves an intermediate that is more stable than the unfolded state and in fact slows down folding relative to protein L, all of which is supported by experiment as well as the coarse-grained model examined here. Perhaps hydrophobic-stabilized intermediates are a concession to certain amino acid sequences, designed by nature for other functional reasons, that would otherwise fold by enthalpic barriers that are simply too high.

Methods

The protein model has been described in (Sorensen & Head-Gordon, 2002; Sorenson & Head-Gordon, 1999; Sorenson & Head-Gordon, 2000; Sorenson & Head-Gordon, 2002). The protein chain is modeled as a sequence of beads of three flavors, hydrophilic, hydrophobic, and neutral, designated by L, B and N, respectively. In general, the pair-wise interaction between beads is attractive for hydrophobic-hydrophobic (B-B) interactions, and repulsive for all

other bead pairs (although the strength of the repulsion interactions depends on the bead types involved). In addition to pair-wise non-bonded interactions, the other contributions to the potential energy function include bending and torsional degrees of freedom. The total potential energy function is given by

$$H = \sum_{\theta} \frac{1}{2} k_\theta (\theta - \theta_0)^2 + \tag{2}$$

$$\sum_{\phi} \left[A(1 + \cos\phi) + B(1 - \cos\phi) + C(1 + \cos 3\phi) + D\left(1 + \cos\left[\phi + \frac{\pi}{4}\right]\right) \right] +$$

$$\sum_{i, j \geq i+3} 4\varepsilon_H S_1 \left[\left(\frac{\sigma}{r_{ij}}\right)^{12} - S_2 \left(\frac{\sigma}{r_{ij}}\right)^6 \right].$$

ε_H determines the energy scale and sets the strength of the hydrophobic interactions. The bond angle energy term is a stiff harmonic potential with force constant $k_\theta = 20\varepsilon_H / rad^2$, and $\theta_0 = 105°$. The second term in the potential energy designates the torsional, or dihedral potential and is given by one of the following: helical (H), with $A = 0$, $B = C = D = 1.2\varepsilon_H$; extended (E), favoring β-strands, with $A = 0.9\varepsilon_H$, $C = 1.2\varepsilon_H$, $B = D = 0$; or turn potential (T), with $A = B = D = 0$, $C = 0.2\varepsilon_H$. For each dihedral angle potential the global minimum is the specified secondary structure type, but has stable local minimum for the other secondary structure angles. This aspect of the potential sits between a Go model and a purely ab initio energy function since the dihedral angle potential is assigned for each bead based on the known native state. However, we use no explicit secondary or tertiary structure template to define any aspect of the potential, and hence the form and parameters are transferable to any protein. The non-bonded interactions are determined by: $S_1 = S_2 = 1$ for B-B interactions; $S_1 = 1/3$ and $S_2 = -1$ for L-L and L-B interactions; and $S_1 = 1$ and $S_2 = 0$ for all N-L, N-B, and N-N interactions. For convenience all simulations are performed in reduced units, with mass m, length σ, energy ε_H, and k_B all set equal to unity. Note that while the non-bonded potential is symmetric with respect to inversion, i.e. $V_{non-bonded}(r_{ij}) = V_{non-bonded}(r_{ji})$, this is not true for the dihedral interactions, as $\phi = f(r_i, r_{i+1}, r_{i+2}, r_{i+3})$. Thus the total energy function is not symmetric with respect to indice permutations.

We perform constant-temperature simulations using Langevin dynamics in the low friction limit for characterizing the thermodynamics and kinetics of folding. Bond lengths are held rigid using the RATTLE algorithm(Andersen, 1983). The free energy landscape is characterized using the multiple, multi-dimensional weighted histogram analysis technique(Ferguson & Garrett, 1999; Ferrenberg & Swendsen, 1989; Kumar et al., 1995). We collect

multi-dimensional histograms over a number of different order parameters, including energy E, radius of gyration R_g, and various native-state similarity parameters χ,

$$\chi = \frac{1}{M} \sum_{i, j \geq i+4}^{N} h\left(\varepsilon - \left| r_{ij} - r_{ij}^{native} \right|\right); \tag{3}$$

where the double sum is over beads on the chain, and r_{ij} and r_{ij}^{native} are the distances between beads i and j in the state of interest and the native state, respectively. h is the Heaviside step function, with $\varepsilon = 0.2$ to account for thermal fluctuations away from the native state structure. M is a constant that satisfies the conditions that $\chi = 1$ when the chain is identical to the native state and $\chi \approx 0$ in the random coil state. The remaining χ parameters are specific to their respective elements of secondary structure. That is, χ_α involves summation over beads in the helix, and $\chi_{\beta 1}$ and $\chi_{\beta 2}$ involve summation over beads in the first β-sheet region and second β-sheet region, respectively, etc.

From the histogram method we get the density of states Ω, as a function of these order parameters, which can be used to calculate thermodynamic quantities. One quantity that is useful is the native-state population as a function of temperature

$$P_{Nat}(T) = \frac{\displaystyle\sum_{\substack{V, R_g, \chi < \chi_{NBA}, \\ \chi_\alpha, \chi_{\beta_1}, \chi_{\beta_2}}} \Omega\left(V, R_g, \chi, \chi_\alpha, \chi_{\beta_1}, \chi_{\beta_2}\right) e^{-V/T}}{\displaystyle\sum_{\substack{V, R_g, \chi, \\ \chi_\alpha, \chi_{\beta_1}, \chi_{\beta_2}}} \Omega\left(V, R_g, \chi, \chi_\alpha, \chi_{\beta_1}, \chi_{\beta_2}\right) e^{-V/T}}$$

$$\tag{4}$$

where χ_{NBA} indicates the boundary of the native-state basin of attraction (NBA) (Nymeyer et al., 1998). In constructing the free energy surfaces we collect histograms at 15 different temperatures: 1.20, 0.90, 0.70, 0.62, 0.60, 0.55, 0.50, 0.48, 0.46, 0.44, 0.42, 0.41, 0.40, 0.39, and 0.38. We run 3 independent trajectories at each temperature, and collect 10,000 data points per trajectory.

The kinetics of the folding process can be characterized by calculating a large number of first-passage times (the time required for a folding trajectory to first enter the native basin of attraction, defined to be $\chi_{NBA} = 0.40$). The first-passage times are calculated by taking an initial high temperature random coil structure and evolving it at the temperature of interest until recording the time that it first enters the native basin of attraction. We subtract off an initial correlation time in which the high-temperature chain is briefly equilibrated at the target temperature (this is the computational dead time during the kinetics run).

To accurately characterize the proper transition-state ensemble in our analysis of protein L and G

Table 4. Sequences for the minimalist models of protein L and G. Differences between the sequences are shown in red.

	Protein L
1°	LBLBLBLBBN NNBBBLBLBB BNNNLLBLLB BLLBNBLBLB LBLNNNLBBL BLBBBL
2°	EEEEEETEH THEEEEEEEE HHEHHHHHHH HHHEHTEEEE EEETTTEEEE EEEE

	Protein G
1°	LBLBLBLBBN NNLBBLBLBB BNNNLLBLLL BLLBNBBBLB BBBNNNLBBL BLBLBL
2°	EEEEEETEH THEEEEEEEE HHEHHHHHHH HHHEHTEEEE EEETTTEEEE EEEE

folding, we employed the P_{fold} method proposed by Du, *et al.*(Du et al., 1998). The method assigns a value, P_{fold}, to a particular structure corresponding to the probability that it will first fold to the native state before unfolding. Structures with P_{fold} values equal to 0.5 correspond to the transition-state ensemble for the model. To apply this method, we first sampled structures from our simulations corresponding to putative transition-state structures. "Putative" transition-state structures were originally isolated by requiring various combinations of order parameters to correspond to their maximum free-energy values in a one-dimensional projection of free energy against these order parameters. From this procedure, an ensemble of structures with $0.4 \leq P_{fold} \leq 0.6$ were isolated during multiple kinetic runs, and were defined as members of the transition state ensemble. By analyzing these structures we are able to postulate new reaction coordinates.

Identifying the transition state ensemble also allowed us to define an intermediate ensemble. By identifying those configurations that have $P_{fold} \approx 0.5$ we can save structures for the trajectories that fail to fold, thus allowing us to postulate an intermediate ensemble. The set of structures obtained in this way can be characterized by analyzing the contacts that are present across all members of the ensemble. Using the defining contacts we can test our definition of intermediates through the direct analysis of kinetic runs. The final test for the validity of any definition of an intermediate ensemble is an analysis performed by fitting to a two-step first order reversible reaction, or UIN mechanism, U ↔ I ↔ N; where U is the unfolded state, I is the intermediate state and N is the native state. The formal solution to this kinetic mechanism is given in Appendix A. The data to which we fit is obtained from simulation by monitoring the progress of the folding trajectories and marking each time a state fits our definition of U, I or N. We note that the kinetic analysis reported by Shimada and Shakhnovich fits the decay of the unfolded population separately from any of the I1, I2 or I3 intermediate populations, i.e. the fit violates mass balance.

Next, we discuss our sequence design procedure. Theoretical work (Bryngelson & Wolynes, 1989; Onuchic et al., 1997; Sali et al., 1994) has elucidated a criterion for heteropolymers to be foldable by noting that there should be a significant energy gap between the native-state and average misfold energies. Our sequence design strategy makes use of this concept. We create a library of misfolds (obtained from simulation of multiple trajectories), and then maximize the energy gap, $\Delta E_{design} = |<E_{misfold}> - E_{native}|$, through favorable mutations on the sequence. We start with a sequence that adopts the protein L/G target topology as given in (Sorenson & Head-Gordon, 2002), and build upon it through sequence mutation to produce new sequences that comprise distinct members, protein L and G, within a target fold class(Brown et al., 2003). The sequence for protein L was determined by aligning it against the real protein L sequence (after mapping the 20-letter code to 3-letter code as described in (Brown et al., 2003)), and proposing new mutations that moved the original sequence towards being more L-like. For protein G, all possible single mutations were investigated during the design process, with the final outcome resulting in the selection of mutations that were beads corresponding to errors in the protein G alignment(Brown et al., 2003). This is interesting in that it appears to hint at potential criteria for performing sequence mapping onto our minimalist code, which could allow for study of novel proteins whose structure is not yet known. Two of the five point mutations for L and G are shared in common (B18L & B47L), which serve to make the proteins more foldable and to clean up certain thermodynamic aspects of the original L/G sequence (Brown et al., 2003). Another 3 mutations are what serve to distinguish the sequence of protein L from that of protein G. Table 4 lists the sequences for L and G used in this study, in which there are a difference of 6 beads between the protein L and G sequences. The energy of the initial L/G sequence is $-32.4\varepsilon_H$, while for the new protein L the native-state energy is $-28.8\varepsilon_H$, and for protein G the native-state energy is $-26.9\varepsilon_H$. For all native states we find that the energy distribution of the misfold library is well separated from the native-state energies.

Finally, we compare the structural similarity of the native state of our protein L model with the experimental structure. The RMSD (root mean square distance) between the native quenched structure of the protein L model and the protein L set of NMR solution structures (2PTL, residues 20-78) was found to be approximately 4.4Å.

10

Appendix A: Solution of UIN mechanism

For the two-step reversible mechanism given in Eq. (1) we have the following differential equations describing the time rate of change in concentration of each species,

$$\frac{d[\text{U}]}{dt} = -k_1[\text{U}] + k_{-1}[\text{I}]$$

$$\frac{d[\text{I}]}{dt} = k_1[\text{U}] - k_{-1}[\text{I}] - k_2[\text{I}] + k_{-2}[\text{N}] \qquad (5)$$

$$\frac{d[\text{N}]}{dt} = k_2[\text{I}] - k_{-2}[\text{N}]$$

These set of coupled first-order differential equations can be straight-forwardly solved by a Laplace transform, given by

$$\mathcal{L}\{\ldots\} = \int_0^\infty \ldots e^{-st} dt \qquad (6)$$

Taking the Laplace transform of the differential equations we have

$$s\mathcal{L}\{[\text{U}]\} - [\text{U}]_0 = -k_1\mathcal{L}\{[\text{U}]\} + k_{-1}\mathcal{L}\{[\text{I}]\}$$

$$s\mathcal{L}\{[\text{I}]\} - [\text{I}]_0 = k_1\mathcal{L}\{[\text{U}]\} - k_{-1}\mathcal{L}\{[\text{I}]\} - k_2\mathcal{L}\{[\text{I}]\} + k_{-2}\mathcal{L}\{[\text{N}]\} \qquad (7)$$

$$s\mathcal{L}\{[\text{N}]\} - [\text{N}]_0 = k_2\mathcal{L}\{[\text{I}]\} - k_{-2}\mathcal{L}\{[\text{N}]\}$$

where $[\text{U}]_0$, $[\text{I}]_0$, and $[\text{N}]_0$ are the initial concentrations at time t = 0. Rearranging gives the set of linear equations

$$(s + k_1)\mathcal{L}\{[\text{U}]\} - k_{-1}\mathcal{L}\{[\text{I}]\} = [\text{U}]_0$$

$$-k_1\mathcal{L}\{[\text{U}]\} + (s + k_2 + k_{-1})\mathcal{L}\{[\text{I}]\} - k_{-2}\mathcal{L}\{[\text{N}]\} = [\text{I}]_0 \qquad (8)$$

$$-k_2\mathcal{L}\{[\text{I}]\} + (s + k_{-2})\mathcal{L}\{[\text{N}]\} = [\text{N}]_0$$

In matrix form these equations can be expressed as

$$\begin{pmatrix} s + k_1 & -k_1 & 0 \\ -k_1 & s + k_{-1} + k_2 & -k_{-2} \\ 0 & -k_2 & s + k_{-2} \end{pmatrix} \begin{pmatrix} \mathcal{L}\{[\text{U}]\} \\ \mathcal{L}\{[\text{I}]\} \\ \mathcal{L}\{[\text{N}]\} \end{pmatrix} = \begin{pmatrix} [\text{U}]_0 \\ [\text{I}]_0 \\ [\text{N}]_0 \end{pmatrix} \qquad (9)$$

For the mechanism we're interested in investigating here, we have the initial conditions that $[\text{I}]_0 = [\text{N}]_0 = 0$. Using Cramer's rule we can express the solutions to the above set of equations (Strang, 1988):

$$\mathcal{L}\{[\text{U}]\} = \frac{\begin{vmatrix} [\text{U}]_0 & -k_1 & 0 \\ 0 & s+k_{-1}+k_2 & -k_{-2} \\ 0 & -k_2 & s+k_{-2} \end{vmatrix}}{\begin{vmatrix} s+k_1 & -k_1 & 0 \\ -k_1 & s+k_{-1}+k_2 & -k_{-2} \\ 0 & -k_2 & s+k_{-2} \end{vmatrix}} \quad (10a)$$

$$\mathcal{L}\{[\text{I}]\} = \frac{\begin{vmatrix} s+k_1 & [\text{U}]_0 & 0 \\ -k_1 & 0 & -k_{-2} \\ 0 & 0 & s+k_{-2} \end{vmatrix}}{\begin{vmatrix} s+k_1 & -k_1 & 0 \\ -k_1 & s+k_{-1}+k_2 & -k_{-2} \\ 0 & -k_2 & s+k_{-2} \end{vmatrix}} \quad (10b)$$

Finding the solutions to the determinants and simplifying gives

$$\mathcal{L}\{[\text{U}]\} = [\text{U}]_0 \left[\frac{(s^2+k_{-1}k_{-2})}{s(s-r_1)(s-r_2)} + \frac{(k_2+k_{-1}+k_{-2})}{(s-r_1)(s-r_2)} \right] \quad (11a)$$

$$\mathcal{L}\{[\text{I}]\} = [\text{U}]_0 \left[\frac{k_1(s+k_{-2})}{s(s-r_1)(s-r_2)} \right]; \quad (11b)$$

where r_1 and r_2 are given by

$$r_1 = -\frac{1}{2}(k_1+k_2+k_{-1}+k_{-2}) \quad (12a)$$
$$+\frac{1}{2}\left[(k_1+k_2+k_{-1}+k_{-2})^2 - 4(k_1k_2+k_1k_{-2}+k_{-1}k_{-2})\right]^{1/2}$$

and

$$r_2 = -\frac{1}{2}(k_1+k_2+k_{-1}+k_{-2}) \quad (12b)$$
$$-\frac{1}{2}\left[(k_1+k_2+k_{-1}+k_{-2})^2 - 4(k_1k_2+k_1k_{-2}+k_{-1}k_{-2})\right]^{1/2}.$$

Taking the inverse Laplace transforms gives us solutions for [U] and [I] as a function of time:

$$[\text{U}] = [\text{U}]_0 \left(\frac{k_{-1}k_{-2}}{r_1 r_2} \right. \quad (13a)$$
$$+ \left[\frac{r_1^2+k_{-1}k_{-2}}{r_1^2-r_1 r_2} + \frac{k_2+k_{-1}+k_{-2}}{r_1-r_2} \right]e^{r_1 t}$$
$$+ \left. \left[\frac{r_2^2+k_{-1}k_{-2}}{r_2^2-r_1 r_2} + \frac{k_2+k_{-1}+k_{-2}}{r_1-r_2} \right]e^{r_2 t} \right)$$

$$[\text{I}] = [\text{U}]_0 k_1 \left(\frac{k_{-2}}{r_1 r_2} + \frac{r_1+k_{-2}}{r_1^2-r_1 r_2}e^{r_1 t} + \frac{r_2+k_{-2}}{r_2^2-r_1 r_2}e^{r_2 t} \right) \quad (13b)$$

The condition of detailed balance gives the final equation for [N],

$$[\text{N}] = [\text{U}]_0 - [\text{U}] - [\text{I}] \quad (14)$$

Thus we obtain solutions for [U], [I], and [N] as functions of time.

References

Abkevich, V. I., Gutin, A. M. & Shakhnovich, E. I. (1994). Specific Nucleus as the Transition State for Protein Folding - Evidence from the Lattice Model. *Biochemistry* **33**(33), 10026-10036.

Alm, E., Morozov, A. V., Kortemme, T. & Baker, D. (2002). Simple physical models connect theory and experiment in protein folding kinetics. *Journal of Molecular Biology* **322**(2), 463-476.

Andersen, H. (1983). Rattle: A "Velocity" Version of the Shake Algorithm for Molecular Dynamics Calculations. *Journal of Computational Physics* **52**, 24-34.

Brown, S., Fawzi, N. J. & Head-Gordon, T. (2003). Coarse-grained sequences for protein folding and design. *Proceedings of the National Academy of Sciences of the United States of America* **100**(19), 10712-10717.

Bryngelson, J. D. & Wolynes, P. G. (1989). Intermediates and Barrier Crossing in a Random Energy Model (with Applications to Protein Folding). *Journal of Physical Chemistry* **V93**(N19), 6902-6915.

Daggett, V. & Fersht, A. (2003a). The present view of the mechanism of protein folding [Review]. *Nature Reviews Molecular Cell Biology* **4**(6), 497-502.

Daggett, V. & Fersht, A. R. (2003b). Is there a unifying mechanism for protein folding? [Review]. *Trends in Biochemical Sciences* **28**(1), 18-25.

Du, R., Pande, V. S., Grosberg, A. Y., Tanaka, T. & Shakhnovich, E. S. (1998). On the transition coordinate for protein folding. *Journal of Chemical Physics* **V108**(N1), 334-350.

Ferguson, D. M. & Garrett, D. G. (1999). Simulated annealing - Optimal histogram methods. *Monte Carlo Methods in Chemical Physics* **105**, 311-336.

Ferrenberg, A. M. & Swendsen, R. H. (1989). Optimized Monte Carlo Data Analysis. *Physical Review Letters* **63**(12), 1195-1198.

Fersht, A. R. (1997). Nucleation mechanisms in protein folding. *Current Opinion in Structural Biology* **7**, 3-9.

Gruebele, M. (2002a). An intermediate seeks instant gratification. *Nature Structural Biology* **V9**(N3), 154-155.

Gruebele, M. (2002b). Protein folding: the free energy surface. *Current Opinion in Structural Biology* **V12**(N2), 161-168.

Gu, H. D., Kim, D. & Baker, D. (1997). Contrasting roles for symmetrically disposed beta-turns in the folding of a small protein. *Journal of Molecular Biology* **V274**(N4), 588-596.

Gu, H. D., Yi, Q. A., Bray, S. T., Riddle, D. S., Shiau, A. K. & Baker, D. (1995). A Phage Display System for Studying the Sequence Determinants of Protein Folding. *Protein Science* **V4**(N6), 1108-1117.

Guo, Z. & Thirumalai, D. (1996). Kinetics and Thermodynamics of Folding of a De Novo Designed Four-Helix Bundle Protein. *Journal of Molecular Biology* **V263**(N2), 323-343.

Guo, Z. Y. & Thirumalai, D. (1995). Kinetics of Protein Folding - Nucleation Mechanism, Time Scales, and Pathways. *Biopolymers* **36**(1), 83-102.

Guo, Z. Y., Thirumalai, D. & Honeycutt, J. D. (1992). Folding Kinetics of Proteins - a Model Study. *Journal of Chemical Physics* **V97**(N1), 525-535.

Head-Gordon, T. & Brown, S. (2003). Minimalist models for protein folding and design. *Current Opinion in Structural Biology* **13**(2), 160-167.

Honeycutt, J. D. & Thirumalai, D. (1990). Metastability of the Folded States of Globular Proteins. *Proceedings of the National Academy of Sciences of the United States of America* **V87**(N9), 3526-3529.

Karanicolas, J. & Brooks, C. L. (2002). The origins of asymmetry in the folding transition states of protein L and protein G. *Protein Science* **11**(10), 2351-2361.

Kim, D. E., Fisher, C. & Baker, D. (2000). A breakdown of symmetry in the folding transition state of protein L. *Journal of Molecular Biology* **298**(5), 971-984.

Krantz, B. A., Mayne, L., Rumbley, J., Englander, S. W. & Sosnick, T. R. (2002). Fast and slow intermediate accumulation and the initial barrier mechanism in protein folding. *Journal of Molecular Biology* **324**(2), 359-371.

Kumar, S., Rosenberg, J. M., Bouzida, D., Swendsen, R. H. & Kollman, P. A. (1995). Multidimensional Free-Energy Calculations Using the Weighted Histogram Analysis Method. *Journal of Computational Chemistry* **V16**(N11), 1339-1350.

McCallister, E. L., Alm, E. & Baker, D. (2000). Critical role of beta-hairpin formation in protein G folding. *Nature Structural Biology* **7**(8), 669-673.

Myers, J. K. & Oas, T. G. (2002). Mechanisms of fast protein folding [Review]. *Annual Review of Biochemistry* **71**, 783-815.

Nauli, S., Kuhlman, B. & Baker, D. (2001). Computer-based redesign of a protein folding pathway. *Nature Structural Biology* **V8**(N7), 602-605.

Nymeyer, H., Garcia, A. E. & Onuchic, J. N. (1998). Folding Funnels and Frustration in Off-Lattice Minimalist Protein Landscapes. *Proceedings of the National Academy of Sciences of the United States of America* **95**(11), 5921-5928.

Onuchic, J. N., LutheySchulten, Z. & Wolynes, P. G. (1997). Theory of protein folding: The energy landscape perspective. *Annual Review of Physical Chemistry* **V48**, 545-600.

Ozkan, S. B., Dill, K. A. & Bahar, I. (2002). Fast-folding protein kinetics, hidden intermediates, and the sequential stabilization model. *Protein Science* **11**(8), 1958-1970.

Park, S. H., Oneil, K. T. & Roder, H. (1997). An early intermediate in the folding reaction of the B1 domain of protein G contains a native-like core. *Biochemistry* **V36**(N47), 14277-14283.

Park, S. H., Shastry, M. C. R. & Roder, H. (1999). Folding dynamics of the B1 domain of protein G explored by ultrarapid mixing. *Nature Structural Biology* **6**(10), 943-947.

Parker, M. J. & Marqusee, S. (1999). The cooperativity of burst phase reactions explored. *Journal of Molecular Biology* **293**(5), 1195-1210.

Plaxco, K. W., Millett, I. S., Segel, D. J., Doniach, S. & Baker, D. (1999). Chain collapse can occur concomitantly with the rate-limiting step in protein folding. *Nature Structural Biology* **V6**(N6), 554-556.

Plaxco, K. W., Simons, K. T. & Baker, D. (1998). Contact order, transition state placement and the refolding rates of single domain proteins. *Journal of Molecular Biology* **V277**(N4), 985-994.

Qin, Z., Ervin, J., Larios, E., Gruebele, M. & Kihara, H. (2002). Formation of a compact structured ensemble without fluorescence signature early during ubiquitin folding. *Journal of Physical Chemistry.*

Sali, A., Shakhnovich, E. & Karplus, M. (1994). How Does a Protein Fold. *Nature* **V369**(N6477), 248-251.

Sanchez, I. E. & Kiefhaber, T. (2003a). Evidence for sequential barriers and obligatory intermediates in apparent two-state protein folding. *Journal of Molecular Biology* **325**(2), 367-376.

==Sanchez, I. E. & Kiefhaber, T. (2003b). Hammond behavior versus ground state effects in protein folding: Evidence for narrow free energy barriers and residual structure in unfolded states. *Journal of Molecular Biology* **327**(4), 867-884.==

Scalley, M. L., Yi, Q., Gu, H. D., McCormack, A., Yates, J. R. & Baker, D. (1997). Kinetics of folding of the IgG binding domain of peptostreptoccocal protein L. *Biochemistry* **V36**(N11), 3373-3382.

Shimada, J. & Shakhnovich, E. I. (2002). The ensemble folding kinetics of protein G from an all-atom Monte Carlo simulation. *Proceedings of the National Academy of Sciences of the United States of America* **V99**(N17), 11175-11180.

Shindyalov, I. N. & Bourne, P. E. (1998). Protein Structure Alignment by Incremental Combinatorial Extension (Ce) of the Optimal Path. *Protein Engineering* **11**(9), 739-747.

Sorensen, J. M. & Head-Gordon, T. (2002). Toward minimalist models of larger proteins: A ubiquitin-like protein. *Proteins-Structure Function and Genetics* **V46**(N4), 368-379.

Sorenson, J. M. & Head-Gordon, T. (1999). Redesigning the hydrophobic core of a model beta-sheet protein: Destabilizing traps through a threading approach. *Proteins-Structure Function and Genetics* **V37**(N4), 582-591.

Sorenson, J. M. & Head-Gordon, T. (2000). Matching simulation and experiment: A new simplified model for simulating protein folding. *Journal of Computational Biology* **V7**(N3-4), 469-481.

Sorenson, J. M. & Head-Gordon, T. (2002). Protein engineering study of protein L by simulation. *Journal of Computational Biology* **V9**(N1), 35-54.

Speed, M. A., Morshead, T., Wang, D. I. C. & King, J. (1997). Conformation of P22 Tailspike Folding and Aggregation Intermediates Probed by Monoclonal Antibodies. *Protein Science* **6**(1), 99-108.

Strang, G. (1988). *Linear Algebra and Its Applications*, Harcourt Brace Jovanovich, Inc.

Wagner, C. & Kiefhaber, T. (1999). Intermediates can accelerate protein folding. *Proceedings of the National Academy of Sciences of the United States of America* **96**(12), 6716-6721.